therefore considered as a relatively benign entity among the astrocytic tumors.[4,8,9] However, 9%–20% of PXAs have been reported to undergo malignant transformation,[10] and some of them exhibit anaplastic features at the first presentation.[11] PXAs with anaplastic features are difficult to manage, and the role of postoperative radiotherapy is not clearly defined.[2,5,12,13] We present a case of PXA with anaplastic features in which we controlled disseminated tumor nodules in the brain and the spinal cord for a relatively long period by repeated stereotactic irradiation (STI).

Case History

A 47-year-old woman presented with an epileptic seizure. CT scanning of the head revealed a 6-cm tumor in the right frontal lobe. MRI showed a well-demarcated, homogeneously enhanced mass lesion accompanied by perifocal edema and midline shift (Fig. 1). The tumor was totally removed, and histological examination revealed a tumor primarily composed of spindle cells with fibrillary cytoplasm (Fig. 2A), arranged in a fascicular pattern. Round or polygonal cells with plumper cytoplasm were admixed, and large pleomorphic cells and multinucleated giant cells were scattered throughout the lesion (Fig. 2B). Reticulin fibers were observed around individual or grouped tumor cells (Fig. 2C). Focally, eosinophilic granular bodies were noted (Fig. 2D). On immunohistochemical examination, tumor cells in some areas were reactive for glial fibrillary acidic protein (Fig. 2E). Cellularity was high, and several mitotic figures were frequently observed. *MIB-1* (mindbomb homolog 1) labeling index was 4% (Fig. 2F). These findings indicated that the tumor was an astrocytic glioma with signs of anaplasia, including high cellularity, increased cellular and nuclear atypia, and focally increased mitotic activity. Histopathological features highly indicative of PXA included cellular pleomorphism, focal eosinophilic protein droplets, and regions with an interstitial reticulin fiber network. A rather solid, noninfiltrative growth of the tumor was also typical with PXA. Furthermore, molecular analysis of the tumor revealed two distinct mutations in exon 4: a missense mutation resulting in an amino acid change at codon 114 (c. 341T>C; L114S) and a nonsense mutation due to a 2-bp deletion (c. 365–366delTG). Both mutations do not correspond to any of the known hotspot mutations typically found in diffuse astrocytic gliomas.[14] Alterations of the *EGFR* (*epidermal growth factor receptor*), *CDK4* (*cyclin-dependent kinase 4*), *MDM2* (*murine double minute 2*), and *CDKN2A* (*cyclin-dependent kinase inhibitor 2A*) genes were not observed, in keeping with what has been reported in the majority of PXAs.[15–17] The histopathological findings together with these molecular analysis results led to the diagnosis of PXA with anaplastic features. The pathological diagnosis was independently confirmed by three neuropathologists.

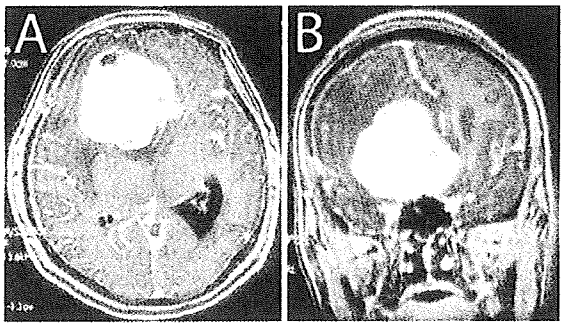

Fig. 1. Axial (A) and coronal (B) gadolinium-enhanced T1-weighted MRI at presentation.

Sixteen months after the first operation, a focal relapse at the primary site was noted and treated with stereotactic radiosurgery (SRS) using Gamma Knife by irradiating 20 Gy at the margin of the tumor (Fig. 3A). Two years later, surgical removal with laminectomy was performed on intrathecal dissemination at the level of the fourth to fifth cervical spine. Histology of this recurrent tumor was analogous to that of the original tumor. However, the recurrent tumor was largely composed of small cells (Fig. 2G), and the MIB-1 labeling index had increased to 10% (Fig. 2H).

At 40 months after the original diagnosis, a new intracranial lesion appeared in the left hypothalamus. Nimustine hydrochloride (100 mg/body) was administered intravenously twice in 2 months, but the lesion showed a poor response to chemotherapy and continued to grow. This lesion was therefore treated by the second SRS using Gamma Knife at 43 months (Fig. 3B). Relapses of several nodular lesions apart from the primary tumor were observed. Spinal cord lesions at the levels of the fourth cervical spine and the fourth thoracic spine were treated with STI at 47 months (Fig. 4A). For this STI, treatment planning with irregularly shaped beams using seven noncoplanar static ports was established with the help of a three-dimensional treatment-planning computer, and the patient was immobilized using a stereotactic body frame. Forty-two Gy in 12 fractions was administered with 6-MV X-rays using a linear accelerator. Newly disseminated lesions in the right temporal lobe and the left cerebellomedullary angle were treated with a third SRS at 50 months (Fig. 3C, D). One month after the third SRS, a spinal cord lesion at the level of the 10th to 12th thoracic spine was partially resected followed by STI delivering 40 Gy in 10 fractions. One dynamic arc instead of multiple static ports was employed for the second STI. At 53 months, temozolomide was administered orally at a dose of 150 mg/m^2 using the 5/28-day protocol, and the patient received six cycles in total. At 55 and 58 months, a fourth and fifth SRS were performed for the lesions in bilateral cerebellar hemispheres (Fig. 3E, F) and the frontal interhemispheric region (Fig. 3G), respectively. At 59 months, the spinal cord lesion at the level of the first to third cervical spine received 35 Gy irradiation in 10 fractions, and another new lesion in the left temporal lobe was treated with a sixth SRS (Fig. 3H).

All of the intracranial lesions treated with SRS and the spinal cord lesions that received STI had successful local

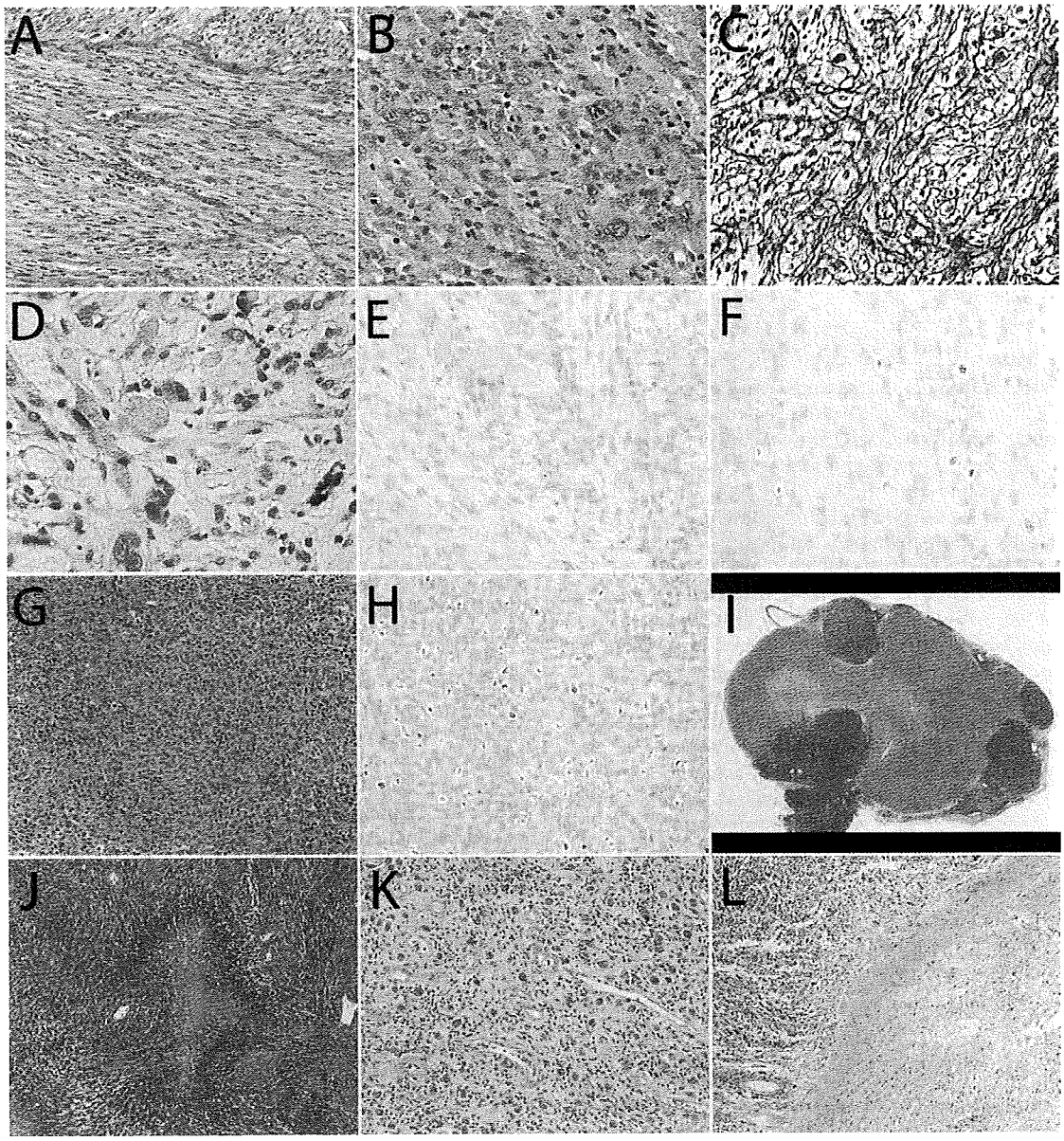

Fig. 2. (A–F) First surgical specimen demonstrating spindle cells (A), pleomorphic cells (B), reticulin fibers (C), eosinophilic protein droplets (D), and cells positive for glial fibrillary acidic protein (E). MIB-1 (mindbomb homolog 1) labeling index was 4% (F). (G and H) Recurrent tumor showing high cellularity (G) and MIB-1 labeling index (H). (I–L) Autopsy specimens showing well-demarcated (I), highly cellular tumor (J) and less cellular region (K) adjacent to degenerated white matter (L). Staining: A, B, D, G, and I–L, hematoxylin and eosin staining; C, silver staining; E, immunostaining for glial fibrillary acidic protein; F and H, MIB-1 staining. Original magnification: A, G, and K, ×200; B, C, E, F, and H, ×400; D, ×800; I, ×10; J and L, ×100.

control (Figs. 4B, 5A–H), and no obvious clinical complications occurred from STI. The patient was free from neurological deficits until the thoracic spinal cord lesion started to cause paraparesis and bladder and bowel dysfunction at 50 months. However, at 60 months, numerous tumor nodules appeared simultaneously throughout the craniospinal axis, which was beyond control by STI. Consciousness deteriorated due to rapid progression of the diffuse dissemination, and she died 66 months after the disease onset.

Autopsy demonstrated multiple disseminated lesions throughout the craniospinal axis. We could not identify the primary lesion. Each disseminated tumor nodule appeared relatively well demarcated from the surrounding brain tissue, although there was marked associated edema (Fig. 2I). Histologically, the specimens were

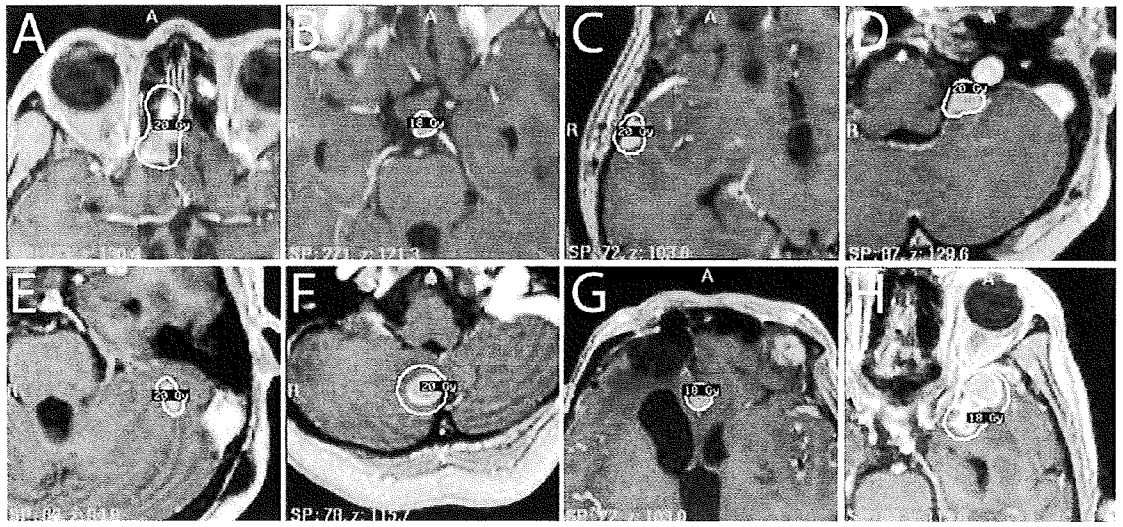

Fig. 3. Treatment planning for the first (A), second (B), third (C and D), fourth (E and F), fifth (G), and sixth (H) SRS.

highly cellular malignant astrocytic tumors with multifocal areas of necrosis and pseudopalisading (Fig. 2J). The tumors grew diffusely within the leptomeninges and in the Virchow-Robin spaces along intracortical vessels. Features characteristic of PXA were no longer present in the disseminated lesions. The lesions treated by SRS were specifically examined. Macroscopically, the irradiated tumors had shrunk and were difficult to recognize. Histological evaluation of these irradiated tumors showed areas with lower cellularity (Fig. 2K), but some areas remained highly cellular, similar to untreated tumors. Irradiated tumors were typically adjacent to degenerated white matter, which probably reflected damage from irradiation (Fig. 2L). In the spinal cord, radionecrotic spots were observed in regions adjacent to the STI-treated lesions (Fig. 4C).

Discussion

Primarily because of the rarity of PXA with anaplastic features,[11,18] the role of standard postoperative therapy for PXA with anaplastic features has not been definitively established. Seventeen cases of PXA showing anaplastic features at the first presentation have been reported.[19] Among 13 patients whose follow-up information was available, five patients died, and the average overall survival was 21 months (range, 1–44 months). For the

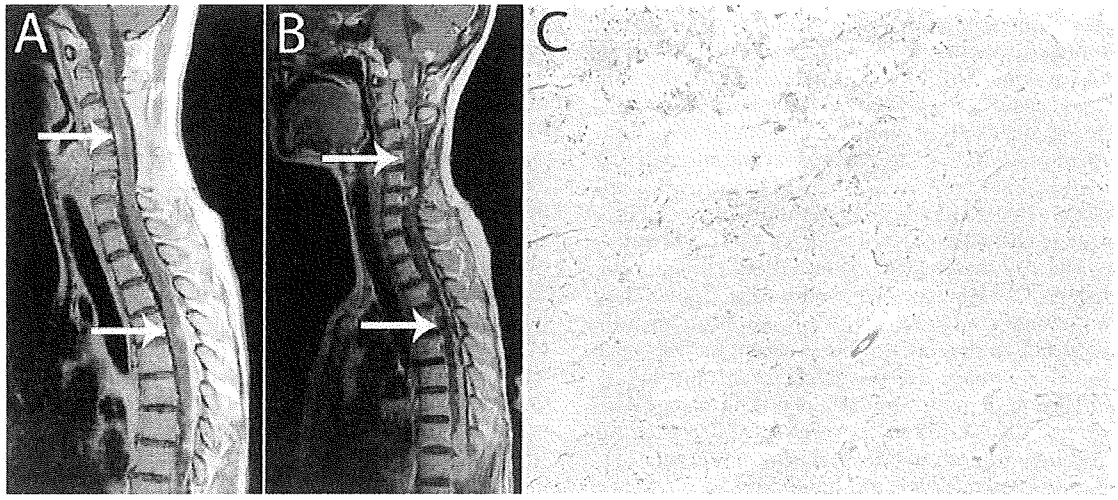

Fig. 4. (A and B) Gadolinium-enhanced T1-weighted MRI of the spinal cord showing lesions before STI (A, white arrows) that were controlled until 60 months (B, white arrows). (C) Autopsy specimen of the spinal cord adjacent to irradiation field showing the area of radiation necrosis (hematoxylin and eosin staining; original magnification, ×50).

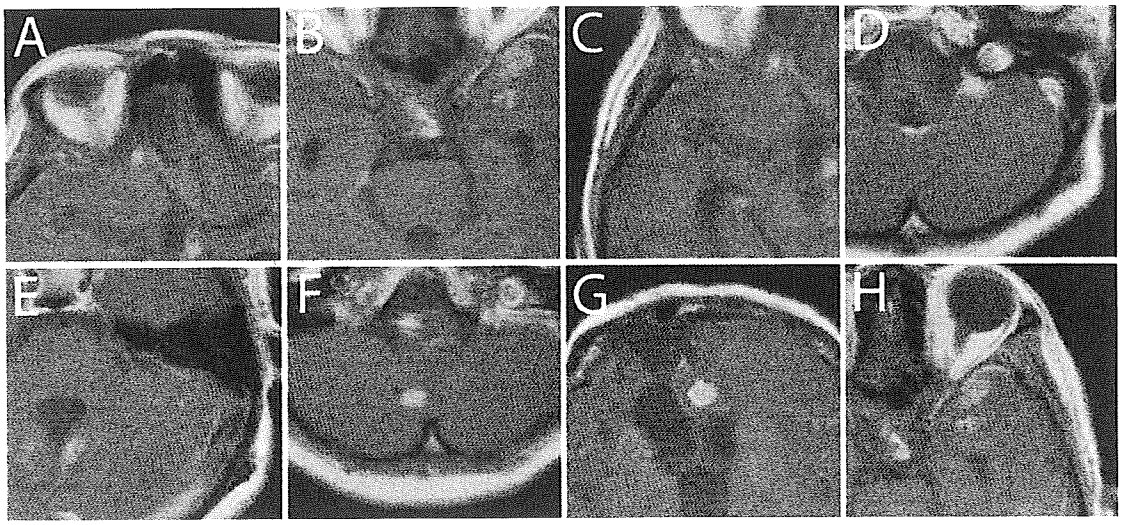

Fig. 5. Gadolinium-enhanced T1-weighted MRI at 60 months. A–H correspond to the lesions treated with SRS shown in Fig. 3A–H.

other eight patients, the last follow-up was at 43 months average (range, 3–144 months).[19] Nine of 17 patients underwent conventional fractionated radiotherapy, but a therapeutic benefit has not been apparent.[19] Notably, in the present case, STI was efficacious in controlling the disseminated nodules of PXA with anaplastic features up to a certain point of progression. By the use of repetitive STI, the patient was free from neurological deficit for 50 months despite frequent tumor recurrences within a short duration. Leptomeningeal dissemination is not an uncommon pattern of recurrence for PXA with anaplastic features and has been observed in two of six recurrent cases.[19] Leptomeningeal dissemination of PXA, with or without anaplastic features, commonly presents as multiple nodular lesions, in contrast to the diffuse dissemination seen in high-grade astrocytomas.[20] Consistently, in the present case, the dissemination caused numerous nodular lesions, but diffuse enhancement of the subarachnoid space was not seen until the last few months. Moreover, at autopsy, the remaining nodules were demonstrated to be well demarcated from the surrounding brain and spinal cord. Such nodular lesions would be amenable to local therapy. In fact, the efficacy of STI for controlling the disseminated nodules was observed by both MRI and histological examinations. In addition, multiple STI treatments were well tolerated, including those to spinal cord lesions, and no complications were noted, although degeneration of adjacent neural tissue was found at autopsy. The use of STI for intramedullary spinal cord malignant tumors has not been reported; however, CyberKnife radiosurgery has been used for spinal benign tumors and arteriovenous malformations and has demonstrated low morbidity.[21,22]

PXA with anaplastic features can show transformation to glioblastoma[7,23] as in the present case; the histology of the disseminated nodules eventually mimicked that of glioblastoma. PXA with anaplastic features at diagnosis typically has a poor prognosis.[11,24] In the present case, the relatively long-term control was obtained by use of STI. The relationship of such control to delaying frankly malignant progression to glioblastoma remains conjectural.

Chemotherapy for PXA has been generally considered ineffective,[2,6] although a case has been reported in which the use of vincristine and carboplatin was effective for controlling bleeding during surgery, presumably due to devascularization.[25] We administered nimustine hydrochloride, according to the regimen for high-grade astrocytoma, and temozolomide, after it became available, but whether these chemotherapeutic reagents contributed to the relatively long survival of the patient is unknown. Rather, the repeated appearance of disseminated nodules during the course of nimustine hydrochloride treatment suggests that the drug was ineffective. Temozolomide was administered only in the late stage of progression, and whether upfront administration of temozolomide is useful awaits further cases; the use of temozolomide for this disease has not been reported previously. Clearly, there is a need for systemic therapy because repeated STI did not cure the disease.

In summary, we present a case of PXA with anaplastic features in which repeated local and distant recurrences were controlled by means of STI for a relatively long period. Whereas conventional chemotherapy and radiotherapy are not curative for PXA with anaplastic features, STI may be a useful therapeutic tool for controlling nodular disseminations and improving quality of life in patients with this disease.

Acknowledgments

We acknowledge Drs. Masahiro Shin and Masao Tago for their participation in radiation therapy.

References

1. Fouladi M, Jenkins J, Burger P, et al. Pleomorphic xanthoastrocytoma: favorable outcome after complete surgical resection. *Neuro-Oncology*. 2001;3:184–192.
2. Giannini C, Scheithauer BW, Burger PC, et al. Pleomorphic xanthoastrocytoma: what do we really know about it? *Cancer*. 1999;85:2033–2045.
3. Gomez JG, Garcia JH, Colon LE. A variant of cerebral glioma called pleomorphic xanthoastrocytoma: case report. *Neurosurgery*. 1985;16:703–706.
4. Kepes JJ, Rubinstein LJ, Eng LF. Pleomorphic xanthoastrocytoma: a distinctive meningocerebral glioma of young subjects with relatively favorable prognosis. A study of 12 cases. *Cancer*. 1979;44:1839–1852.
5. Cervoni L, Salvati M, Santoro A, Celli P. Pleomorphic xanthoastrocytoma: some observations. *Neurosurg Rev*. 1996;19:13–16.
6. Thomas C, Golden B. Pleomorphic xanthoastrocytoma: report of two cases and brief review of the literature. *Clin Neuropathol*. 1993;12:97–101.
7. Whittle IR, Gordon A, Misra BK, Shaw JF, Steers AJ. Pleomorphic xanthoastrocytoma. Report of four cases. *J Neurosurg*. 1989;70:463–468.
8. Stuart G, Appleton DB, Cooke R. Pleomorphic xanthoastrocytoma: report of two cases. *Neurosurgery*. 1988;22:422–427.
9. Giannini CPW, Louis DN, Liberski P. Pleomorphic xanthoastrocytoma. In: Louis DN, Ohgaki H, Wiestler OD, Cavenee WK, eds. *World Health Organization Classification of Tumours of the Central Nervous System*. 4th ed. Lyon, France: International Agency for Research on Cancer; 2007;22–24.
10. Chakrabarty A, Mitchell P, Bridges LR, Franks AJ. Malignant transformation in pleomorphic xanthoastrocytoma—a report of two cases. *Br J Neurosurg*. 1999;13:516–519.
11. Lubansu A, Rorive S, David P, et al. Cerebral anaplastic pleomorphic xanthoastrocytoma with meningeal dissemination at first presentation. *Childs Nerv Syst*. 2004;20:119–122.
12. Bayindir C, Balak N, Karasu A, Kasaroglu D. Anaplastic pleomorphic xanthoastrocytoma. *Childs Nerv Syst*. 1997;13:50–56.
13. Bucciero A, De Caro MI, Tedeschi E, et al. Atypical pleomorphic xanthoastrocytoma. *J Neurosurg Sci*. 1998;42:153–157.
14. Koga H, Zhang S, Kumanishi T, et al. Analysis of p53 gene mutations in low- and high-grade astrocytomas by polymerase chain reaction-assisted single-strand conformation polymorphism and immunohistochemistry. *Acta Neuropathol*. 1994;87:225–232.
15. Weber RG, Hoischen A, Ehrler M, et al. Frequent loss of chromosome 9, homozygous CDKN2A/p14(ARF)/CDKN2B deletion and low TSC1 mRNA expression in pleomorphic xanthoastrocytomas. *Oncogene*. 2007;26:1088–1097.
16. Kaulich K, Blaschke B, Numann A, et al. Genetic alterations commonly found in diffusely infiltrating cerebral gliomas are rare or absent in pleomorphic xanthoastrocytomas. *J Neuropathol Exp Neurol*. 2002;61:1092–1099.
17. Paulus W, Lisle DK, Tonn JC, et al. Molecular genetic alterations in pleomorphic xanthoastrocytoma. *Acta Neuropathol*. 1996;91:293–297.
18. Hirose T, Ishizawa K, Sugiyama K, Kageji T, Ueki K, Kannuki S. Pleomorphic xanthoastrocytoma: a comparative pathological study between conventional and anaplastic types. *Histopathology*. 2008;52:183–193.
19. Marton E, Feletti A, Orvieto E, Longatti P. Malignant progression in pleomorphic xanthoastrocytoma: personal experience and review of the literature. *J Neurol Sci*. 2007;252:144–153.
20. Nakajima T, Kumabe T, Shamoto H, Watanabe M, Suzuki H, Tominaga T. Malignant transformation of pleomorphic xanthoastrocytoma. *Acta Neurochir (Wien)*. 2006;148:67–71.
21. Dodd RL, Ryu MR, Kamnerdsupaphon P, Gibbs IC, Chang SD Jr, Adler JR Jr. CyberKnife radiosurgery for benign intradural extramedullary spinal tumors. *Neurosurgery*. 2006;58:674–685.
22. Sinclair J, Chang SD, Gibbs IC, Adler JR Jr. Multisession CyberKnife radiosurgery for intramedullary spinal cord arteriovenous malformations. *Neurosurgery*. 2006;58:1081–1089.
23. Kepes JJ, Rubinstein LJ, Ansbacher L, Schreiber DJ. Histopathological features of recurrent pleomorphic xanthoastrocytomas: further corroboration of the glial nature of this neoplasm. A study of 3 cases. *Acta Neuropathol*. 1989;78:585–593.
24. Hirose T, Giannini C, Scheithauer BW. Ultrastructural features of pleomorphic xanthoastrocytoma: a comparative study with glioblastoma multiforme. *Ultrastruct Pathol*. 2001;25:469–478.
25. Cartmill M, Hewitt M, Walker D, Lowe J, Jaspan T, Punt J. The use of chemotherapy to facilitate surgical resection in pleomorphic xanthoastrocytoma: experience in a single case. *Childs Nerv Syst*. 2001;17:563–566.

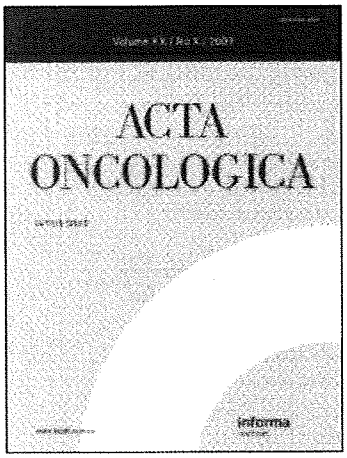

Acta Oncologica
Publication details, including instructions for authors and subscription information:
http://www.informaworld.com/smpp/title~content=t713690780

Quality assurance of volumetric modulated arc therapy using Elekta Synergy

Akihiro Haga [a]; Keiichi Nakagawa [a]; Kenshiro Shiraishi [a]; Saori Itoh [a]; Atsuro Terahara [a]; Hideomi Yamashita [a]; Kuni Ohtomo [a]; Shigeki Saegusa [a]; Toshikazu Imae [a]; Kiyoshi Yoda [b]; Roberto Pellegrini [c]
[a] Department of Radiology, University of Tokyo Hospital, Tokyo, Japan [b] Elekta KK, Kobe, Japan [c] Elekta, Milano, Italy

To cite this Article Haga, Akihiro, Nakagawa, Keiichi, Shiraishi, Kenshiro, Itoh, Saori, Terahara, Atsuro, Yamashita, Hideomi, Ohtomo, Kuni, Saegusa, Shigeki, Imae, Toshikazu, Yoda, Kiyoshi and Pellegrini, Roberto'Quality assurance of volumetric modulated arc therapy using Elekta Synergy', Acta Oncologica, 48: 8, 1193 — 1197
To link to this Article: DOI: 10.3109/02841860903081905
URL: http://dx.doi.org/10.3109/02841860903081905

Acta Oncologica, 2009; 48: 1193–1197

informa
healthcare

ORIGINAL ARTICLE

Quality assurance of volumetric modulated arc therapy using Elekta Synergy

AKIHIRO HAGA[1], KEIICHI NAKAGAWA[1], KENSHIRO SHIRAISHI[1], SAORI ITOH[1], ATSURO TERAHARA[1], HIDEOMI YAMASHITA[1], KUNI OHTOMO[1], SHIGEKI SAEGUSA[1], TOSHIKAZU IMAE[1], KIYOSHI YODA[2] & ROBERTO PELLEGRINI[3]

[1]*Department of Radiology, University of Tokyo Hospital, 7-3-1 Hongo, Bunkyo-ku, Tokyo 113-8655 Japan,* [2]*Elekta KK, Kobe, Japan and* [3]*Elekta, 3D Line, Milano, Italy*

Abstract

Purpose. Recently, Elekta has supplied volumetric modulated arc therapy (VMAT) in which multi-leaf collimator (MLC) shape, jaw position, collimator angle, and gantry speed vary continuously during gantry rotation. A quality assurance procedure for VMAT delivery is described. *Methods and materials.* A single-arc VMAT plan with 73 control points (CPs) and 5-degree gantry angle spacing for a prostate cancer patient has been created by ERGO++ treatment planning system (TPS), where MLC shapes are given by anatomic relationship between a target and organs at risk and the monitor unit for each CP is optimized based on given dose prescriptions. Actual leaf and jaw positions, gantry angles and dose rates during prostate VMAT delivery were recorded in every 0.25 seconds, and the errors between planned and actual values were evaluated. The dose re-calculation using these recorded data has been performed and compared with the original TPS plan using the gamma index. *Results.* Typical peak errors of gantry angles, leaf positions, and jaw positions were 3 degrees, 0.6 mm, and 1 mm, respectively. The dose distribution obtained by the TPS plan and the recalculated one agreed well under 2%-2 mm gamma index criteria. *Conclusions.* Quality assurance for prostate VMAT delivery has been performed with a satisfied result.

The concept of volumetric modulated arc therapy (VMAT) originated from the conformal avoidance radiation therapy [1] with a dynamical movement of MLC while rotating the gantry. By modulating beam intensity during the gantry rotation, intensity modulated arc therapy (IMAT) was proposed and further investigated [2–6]. VMAT is one of the techniques to realize IMAT by varying gantry speed and dose rate with dynamical movement of MLC and jaw [7]. Recently, this has been clinically available [8–10] and a combination of Elekta Synergy with the latest linac control software and ERGO++ treatment planning system (TPS) is one example.

The purpose of this paper is to investigate how much error is caused in dose distribution due to the fluctuation in the dynamical parameters. The linac controller in Elekta Synergy (Elekta, Crawley, UK), RT Desktop 7.0.1, serves to record measured data of dose rates, gantry angles, MLC and jaw positions with 0.25 s interval during VMAT treatment. We can evaluate the influence of these errors by recalculating the dose distribution with these actual dynamical parameters. Since this is an independent simulation analysis and therefore we may be able to specify the cause when VMAT film verification failed.

Methods and materials

A single-arc VMAT plan for prostate cancer was created by ERGO++ v1.71 TPS (Elekta/3DLine, Milano) with D95 prescription (dose to 95% of target volume) of 76 Gy in 38 fractions. A single arc was discretized into 73 static beams or CPs placed at 5-degree gantry angle intervals between −175 and +175 degrees and the first and last CPs were positioned at −179 and +179 degrees (Figure 1). The field shape for each control point was determined by either conformal or conformal avoidance strategy with a 6 mm leaf margin to Planning Target Volume (PTV). In other words, the rectum was

Correspondence: Akihiro Haga, Department of Radiology, University of Tokyo Hospital, 7-3-1 Hongo, Bunkyo-ku, Tokyo 113-8655 Japan. Tel: +81 3 5800 9002. Fax: +81 3 5800 8786. E-mail: haga-haga@umin.ac.jp

(Received 5 April 2009; accepted 30 May 2009)

ISSN 0284-186X print/ISSN 1651-226X online
DOI: 10.3109/02841860903081905

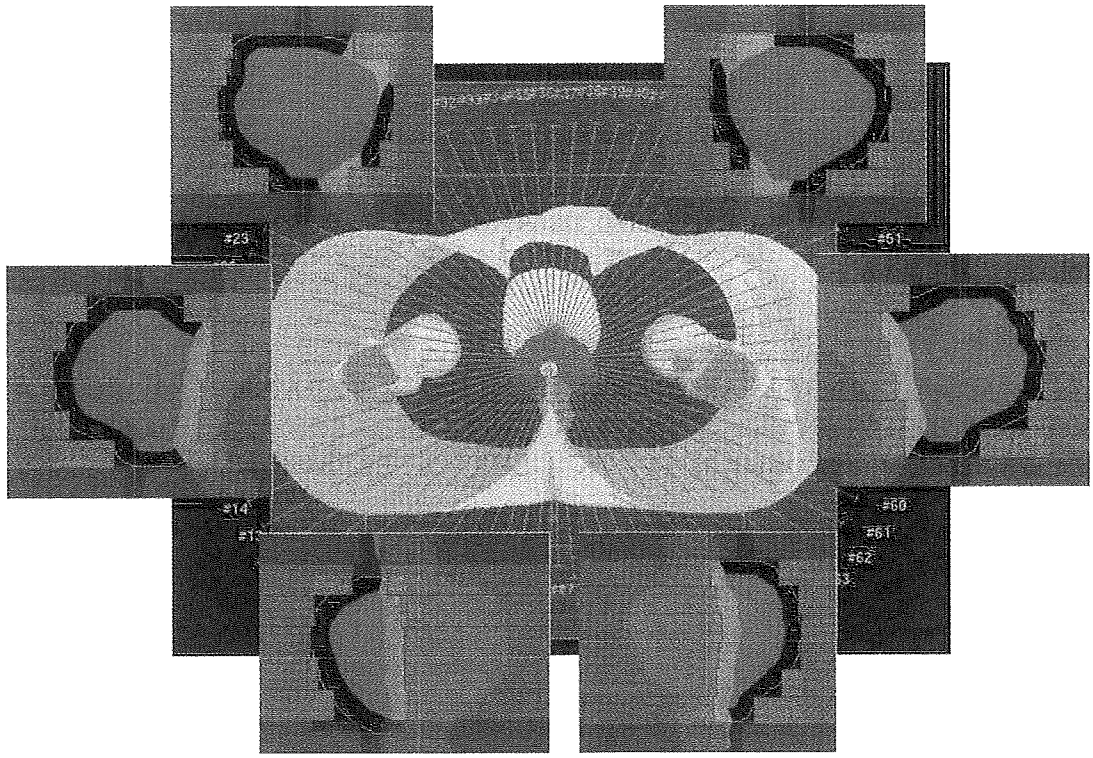

Figure 1. A single-arc VMAT plan with 73 CPs and 5-degree gantry angle spacing for a prostate cancer patient has been created by ERGO++ treatment planning system, where MLC shapes are given by anatomies of target and organs at risk and monitor units for each CP is optimized by simulated annealing algorithm based on given dose prescriptions. The red and pink regions are PTV and rectum, respectively.

partially shielded by MLC when it was in front of the target in beam's eye view, while the whole target was irradiated when it was in front of the rectum.

In the present study, the collimator angle was fixed at 180 degrees. Beam weights for all CPs were optimized by inverse planning based on the simulated annealing algorithm. Dose grid resolution was 2 mm × 2 mm × 2 mm for 3D calculation. After inverse planning, the CPs were grouped into a single arc with the VMAT sequencer in ERGO++ TPS, where a monitor unit (MU) to be delivered between two adjacent CPs was calculated by adding MUs at the two adjacent CPs and then multiplied by 0.5. The created plan was sent to MOSAIQ v1.6 (Elekta IMPAC, USA), and then delivered by the RT desktop controller.

For dose verification, VMAT plan was transferred to two phantom studies. One was a cylindrical water phantom with 0.015 cc pin-point ionization chamber (Type 31014, PTW, Germany) placed at the isocentre. The other was a pelvic water phantom including a GafChromic film (International Specialty Products, NJ, USA) to measure the dose distribution on axial, coronal, and sagittal planes including the isocentre. The GafChromic film was scanned using a flatbed scanner (EPSON GT-X770, Japan) and the gamma index with 3% of a dose at the measurement point and 3 mm has been evaluated by using DD-system v9.0 (R-tech, Japan).

The linac controller in service mode was capable of recording the actual gantry angle, MLC and jaw positions, and dose rate as a function of time. The MLC and jaw positions in each CP computed by ERGO++ were compared with the corresponding measured values. The cumulative MU error is practically negligible because Elekta VMAT delivery is based on MU-based servo control. Instead, the gantry angle error is discussed, which is defined as the difference between the gantry angle for each CP and the gantry angle where a cumulative MU reaches a specified value. A gantry speed dependence of these errors with the same VMAT plan was also examined by employing two times slower gantry speed than a commonly used clinical speed.

Using the actual data of gantry angle, MLC and jaw positions, and the cumulative MUs, dose distribution was re-calculated using Pinnacle v7.4i TPS (Philips, USA), and the dose in the original plan transferred into Pinnacle was compared with the re-calculated dose distribution.

Results

The beam-on time was typically 100 s for a single-arc prostate VMAT delivery. The isocentre dose discrepancy between plans and measurements for 17 patients was $-0.5 \pm 0.8\%$ (s.d.). The averages of the pass rate with a gamma criteria of 3 mm and 3% of a dose at the measurement point were 97.3%, 91.8%, and 92.2% on axial, sagittal, and coronal planes for a region having a dose greater than 30% of the isocentre dose, respectively.

Figure 2 demonstrates measured errors between planned and actual gantry angles during VMAT delivery for three consecutive runs. The red data points show the position errors for a normal delivery time of 100 s, whereas the blue data points show those for a delivery time of 200 s. The bar shows the error range for the three runs. The gantry angle ranges of zero gantry angle error were due to move-only control points with no dose delivery.

Figure 3a and b show measured errors between planned and actual leaf positions during VMAT delivery for three consecutive runs of the same VMAT plan as in Figure 2. Figure 3a depicts a position error of right leaf number 20, which is one of the centre leaves, whereas Figure 3b depicts a position error of left leaf number 20. Again the red data points show the position errors for a normal delivery time of 100 s, whereas the blue data points show those for a delivery time of 200 s. The bar shows the error range for the three runs. The gantry angle ranges of zero leaf error were due to move-only control points with no dose delivery.

Figure 4a and b depicts measured errors between planned and actual X1 and X2 back-up jaw positions, respectively, during VMAT delivery for three consecutive runs of the same VMAT plan. Once again, the red data points show the position errors for a normal delivery time of 100 s, whereas the blue data points show those for a delivery time of

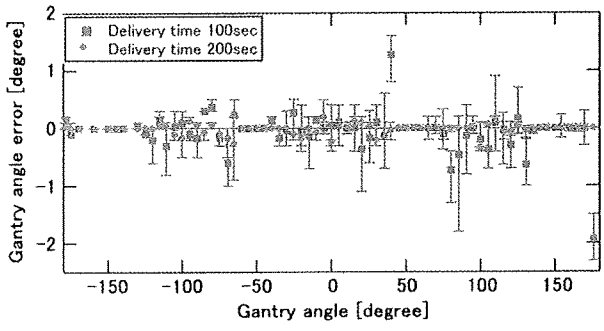

Figure 2. Measured errors between planned and actual gantry angles for three consecutive runs of the same VMAT plan. The red data points show the position errors for a normal delivery time of 100 s, whereas the blue data points show those for a delivery time of 200 s. The bar shows the error range for the three runs.

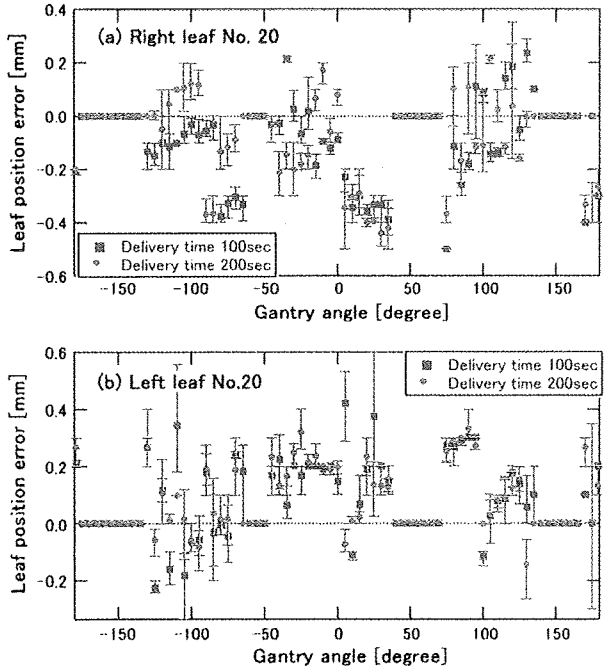

Figure 3. Measured errors between planned and actual leaf positions of the two centre leaves for three consecutive runs of the same VMAT plan: (a) position error of right leaf number 20, (b) position error of left leaf number 20. Again the red data points show the position errors for a normal delivery time of 100 s, whereas the blue data points show those for a delivery time of 200 s. The bar shows the error range for the three runs. The gantry angle ranges of zero leaf error were due to move-only control points with no dose delivery.

200 s. The bar shows the error range for the three runs. The gantry angle ranges of zero back-up jaw error were due to move-only control points with no dose delivery.

Figure 5a and b show gamma-index comparisons between an ERGO++ plan and re-calculated dose using actual data of MLC and jaw positions, gantry angles, and MUs with an interval of every 1 s. The red areas indicate gamma indices of larger than one under criteria of (a) 2% of a dose at the calculated point and 2 mm and (b) 1% of a dose at the calculated point and 1 mm.

Discussion

We have shown highly accurate prostate VMAT delivery using Elekta Synergy and ERGO++ TPS. While the dose agreement in the isocentre shows that total MU is correctly delivered, the agreement of dose distribution on axial, sagittal, and coronal planes assures accurate VMAT delivery. In the Synergy control system, the MLC, jaw, and gantry speed are servo-controlled based on cumulative MUs in each CP. Hence the errors in such dynamical parameters are quickly compensated by

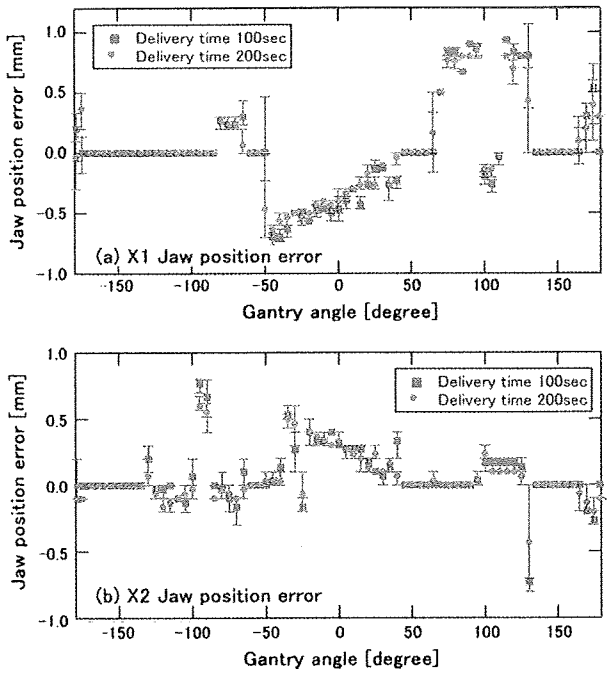

Figure 4. Measured errors between planned and actual back-up jaw positions for three consecutive runs of the same VMAT plan: (a) position error of X1 jaw, (b) position error of X2 jaw. Once again the red data points show the position errors for a normal delivery time of 100 s, whereas the blue data points show those for a delivery time of 200 s. The bar shows the error range for the three runs. The gantry angle ranges of zero back-up jaw error were due to move-only control points with no dose delivery.

real-time feedback control. For instance, it was found that the gantry angle error was immediately corrected as seen in Figure 2. In addition to the mechanical control, it is very important to mention that ERGO++ creates the MLC shape based on the anatomy relationship between the target and organs at risk from the beams eye view. Since it is a smooth function of gantry angle, no major changes are observed in MLC and jaw positions between adjacent control points thereby leading to more accurate dose calculation in TPS.

In the present work, the errors in gantry angles, MLC and jaw positions during VMAT delivery were analyzed. As seen in Figures 2–4, these errors were reproduced among three consecutive runs of the same VMAT plan, and were considered to be caused by accelerations of gantry, leaves, and jaws, which were required in almost the same gantry angles. In fact, it was clearly observed that the gantry angle error decreased when the gantry speed was slower as shown in Figure 2. In principle, smaller leaf and jaw position errors can be anticipated when the gantry speed is slower due to lower leaf and jaw speeds. In the present prostate plan which has no large leaf and jaw movements during gantry rotation, the leaf and back-up jaw position errors were comparable between two different delivery times. Instead, error tolerances of leaf and jaw positions given in the radiation control system may be a major cause of the observed errors.

As shown in Figure 5, the influence of these dynamical errors was negligible under criteria of 2% of a dose at the calculated point and 2 mm. Even under 1% of a dose at the calculated point and 1 mm criteria, the result was good except for low dose region. In other words, the errors in the dynamical parameters with the observed orders in prostate VMAT delivery do not affect the resulting dose distribution significantly.

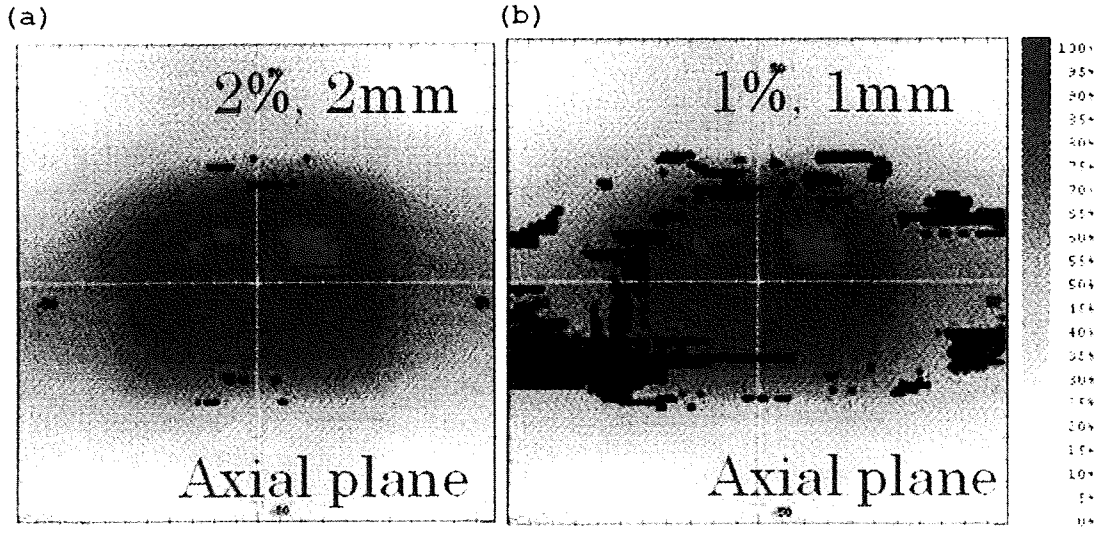

Figure 5. Gamma comparison between an ERGO++ plan and re-calculated dose using actual data of MLC and jaw positions, gantry angles, and MUs with an interval of every 1 s. The red areas indicate gamma indices of larger than one under criteria of (a) 2% of a dose at the calculated point and 2 mm and (b) 1% of a dose at the calculated point and 1 mm.

Conclusion

VMAT dose measurement for prostate cancer agreed well with the plan created by ERGO++. The observed errors of the dynamical parameter did not affect the dose distribution significantly. Quality assurance for prostate VMAT plans has been performed with a satisfied result.

Declaration of interest: Dr. Nakagawa receives research funding from Elekta KK.

References

[1] Takahashi S. Conformation radiotherapy: Rotation techniques as applied to radiography and radiotherapy of cancer. Acta Radiol Suppl 1965;242:1–142.

[2] Yu CX. Intensity-modulated arc therapy with dynamic multileaf collimation: An alternative to tomotherapy. Phys Mod Biol 1995;40:1435–49.

[3] Yu CX, Li XA, Ma I, et al. Clinical implementation of intensity modulated arc therapy. Int J Radiat Oncol Biol Phys 2002;53:453–6.

[4] Earl MA, Shepard DM, Maqvi SA, et al. Intensity modulated arc therapy simplified. Int J Radiat Oncol Biol Phys 2002;53:222–35.

[5] Earl MA, Shepard DM, Maqvi SA, et al. Inverse planning for intensity modulated arc therapy using direct aperture optimization. Phys Med Biol 2003;48:1075–89.

[6] Shepard DM, Cao D, Afghan MKN, Earl MA. An arc-sequencing algorithm for intensity modulated arc therapy. Med Phys 2007;34:464–70.

[7] Otto K. Volumetric modulated arc therapy: IMRT in a single gantry arc. Med Phys 2008;35:310–7.

[8] Bedford JL, Nordmark HV, MacNair HA, Aitken AH, Brock JE, et al. Treatment of lung cancer using volumetric modulated arc therapy and image guidance: A case study. Acta Oncol 2008;47:1438–43.

[9] Bedford JL, Warrington AP. Commissioning of volumetric modulated arc therapy (VMAT). Int J Radiat Oncol Biol Phys 2009;73:537–45.

[10] Korrenman S, Medin J, Kristoffersen FK. Dosimetric verification of RapidArc treatment delivery. Acta Oncol 2009;48:185–91.

Radiotherapy and Oncology 91 (2009) 433–437

Contents lists available at ScienceDirect

Radiotherapy and Oncology

journal homepage: www.thegreenjournal.com

Lung cancer RT

Relation between elective nodal failure and irradiated volume in non-small-cell lung cancer (NSCLC) treated with radiotherapy using conventional fields and doses

Naoko Sanuki-Fujimoto [a,*], Minako Sumi [a], Yoshinori Ito [a], Atsushi Imai [a], Yoshikazu Kagami [a], Ikuo Sekine [b], Hideo Kunitoh [b], Yuichiro Ohe [b], Tomohide Tamura [b], Hiroshi Ikeda [a]

[a] Department of Radiation Oncology, National Cancer Center Hospital, Japan
[b] Department of Thoracic Oncology and Internal Medicine, National Cancer Center Hospital, Japan

ARTICLE INFO

Article history:
Received 3 October 2008
Received in revised form 29 December 2008
Accepted 30 December 2008
Available online 21 January 2009

Keywords:
Chemoradiotherapy
Elective nodal failure
Elective nodal irradiation
Non-small-cell lung carcinoma
Radiotherapy

ABSTRACT

Introduction: The role of elective nodal irradiation of non-small-cell lung cancer (NSCLC) patients treated with radiotherapy remains unclear. We investigated the significance of treating clinically uninvolved lymph nodes by retrospectively analyzing the relationship between loco-regional failure and the irradiated volume.

Methods: Between 1998 and 2003, patients with IA–IIIB NSCLC were treated with radiotherapy. The eligibility criteria for this study were an irradiation dose of 60 Gy or more and a clinical response better than stable disease. Typical radiotherapy consisted of 40 Gy/20 fr to the tumor volumes (clinical target volume of the primary tumor [CTVp], of the metastatic lymph nodes [CTVn], and of the subclinical nodal region [CTVs]), followed by off-cord boost to CTVp+n to a total dose 60–68 Gy/30–34 fr. The relationship between the sites of recurrence and irradiated volumes was analyzed.

Results: A total of 127 patients fulfilled the eligibility criteria. Their median overall and progression-free survival times were 23.5 (range, 4.2–109.7) and 9.0 months (2.2–109.7), respectively. At a median follow-up time of 50.5 months (range, 14.2–83.0) for the surviving patients, the first treatment failure was observed in 95 patients (loco-regional; 41, distant; 42, both; 12). Among the patients with loco-regional failure, in-field recurrence occurred in 38 patients, and four CTVs recurrences associated with CTVp+n failure were observed. No isolated recurrence in CTVs was observed.

Conclusions: In-field loco-regional failure, as well as distant metastasis, was a major type of failure, and there was no isolated elective nodal failure. Radiation volume adequacy did not seem to affect elective nodal failure.

 Radiotherapy and Oncology 91 (2009) 433–437

Radiation therapy is an integral component of the multi-modal treatment of non-small-cell lung cancer (NSCLC). Recent phase III studies have demonstrated that concomitant chemoradiotherapy improves survival, and this has resulted in the general acceptance of concurrent chemoradiotherapy as one of the standard treatments for locally advanced NSCLC [1]. Despite the improved survival, however, most patients die from their disease as a result of local or distant failure.

Local failure remains a major challenge when treating NSCLC with radiotherapy. A number of studies of dose escalation to the gross tumor volume (GTV) have been conducted as a means of improving local control [2–5]. The conventional radiation fields for NSCLC typically encompass the entire mediastinum and ipsilateral hilum (elective nodal region) to deliver a dose of 40 Gy, even without evidence of disease in these areas, followed by a 20 Gy boost to the GTV. However, the conventional treatment has added considerable morbidity and can limit the dose escalation. In phase I–II dose escalation studies, there is a trend toward omitting the practice of elective nodal irradiation (ENI) after their experiences with toxicity, which is not based on direct evidence [2–5]. According to those studies, omitting ENI has not sacrificed treatment outcomes so far. They also analyzed patterns of recurrence in relation to irradiated volume in a dose escalation setting [6].

By contrast, the current literature provides limited information regarding patterns of failure when conventional fields and doses are used [7,8]. Since it is important to know whether loco-regional failure is within or outside the irradiation field, we retrospectively analyzed patterns of failure after radiation therapy for NSCLC, especially in regard to the relationship between local failure and irradiated volume.

Methods and materials

Patients

Between January 1998 and March 2003, 263 patients with newly diagnosed NSCLC were treated with thoracic radiation therapy,

* Corresponding author. Address: Department of Radiation Oncology, National Cancer Center Hospital, 1-1, Tsukiji 5-chome, Chuo-ku, Tokyo 104-0045, Japan.
E-mail address: nao5-tky@umin.ac.jp (N. Sanuki-Fujimoto).

0167-8140/$ - see front matter
doi:10.1016/j.radonc.2008.12.013

with or without chemotherapy, at the National Cancer Center Hospital. All tumors were cytologically or histologically confirmed NSCLC. Patients' disease was staged by the tumor-node-metastasis (TNM) staging system (UICC, version 6, 2002). The diagnostic workup included a bone scan, brain scan by computed tomography (CT) or magnetic resonance imaging, CT scan of the chest, and CT or ultrasound imaging of the abdomen. The criteria for inclusion in this study were irradiation with a dose of 60 Gy or more as a part of the initial treatment and a clinical response better than stable disease. After excluding patients with metastatic disease, whose primary tumor was located in the apex of the lung (superior sulcus), and whose post-treatment evaluation was inadequate, the remaining 127 patients served as the subjects of the analysis.

Details of treatment

Radiotherapy

Gross tumor volume (GTV) was defined as the demonstrable extent of the primary tumor and the metastatic lymph nodes, GTVp and GTVn, respectively. GTVn was defined as abnormally enlarged regional lymph nodes measuring over 1.0 cm along their short axis. Clinical target volume (CTV) consisted of the adjacent mediastinum and ipsilateral hilum (CTV of the subclinical nodal region, CTVs) as well as CTVp and CTVn which were assumed to be equal to GTVp and GTVn, respectively. A planning target volume (PTV) margin of 1–1.5 cm was drawn around each CTV.

External-beam radiotherapy with a 6, 10, or 15 MV photon beam was delivered using a linear accelerator. A majority of the patients were treated with anteroposterior opposing fields encompassing CTV to a dose of 40 Gy/20 fractions (2 Gy per fraction, 5 days per week), followed by an off-cord boost to the GTV by oblique opposing fields, to a total dose of 60–68 Gy/30–34 fractions. No attempt was made to encompass the supraclavicular areas in most patients; the supraclavicular areas were treated only electively. Initially, treatment planning was performed by using an X-ray simulator for the anteroposterior fields and a CT-port for the oblique opposing fields, but after the end of 1999, most treatment planning, especially to define the off-cord boost, was performed using a CT-based planning system (FOCUS, Computed Medical Systems).

The dose to the spinal cord was limited to 45–50 Gy. The size of the treatment fields was adjusted so that it did not exceed half of the hemithorax before introducing CT-based planning system, or so that the volume of normal lung tissue receiving a dose over 20 Gy would be less than 40%.

Chemotherapy

Systemic chemotherapy was used in 87 patients (68.5%), and the majority of the patients received platinum-based chemotherapy sequentially or concurrently with the radiation therapy. One of the representative regimens was 2–3 cycles of cisplatin 80 mg/sqm on day 1 and vinorelbine 25 mg/sqm on days 1 and 8 (or vindesine 3 mg/sqm on days 1, 8, and 15) in 21–28 days. The second most common regimen was cisplatin 80 mg/sqm on day 1, vindesine 3 mg/sqm on days 1 and 8, and mitomycin C 8 mg/sqm on day 1, in 21–28 days. The other regimens are summarized in Table 1.

Evaluation

Patients were followed at 4- to 6-week intervals for 6 months after treatment and at 3- to 6-month intervals thereafter. Chest X-ray and laboratory workups were performed at each post-treatment visit. Unless there were changes in the chest X-ray or in symptoms, a CT scan was performed about 2–3 months after the treatment for the assessment of the treatment response, and every 6–12 months thereafter. Follow-up information was obtained from the medical charts and death certificates.

Table 1
Baseline patient characteristics.

Characteristics	Patients	(%)
Median age (yr)	65 (36–83)	
Gender		
Male	106	83
Female	21	17
Performance status (WHO)		
0	12	9
1	109	86
2	6	5
Stage		
I (A/B)	5(1/4)	4
II (A/B)	12(3/9)	9
III (A/B)	110(59/51)	87
Histology		
Adenocarcinoma	64	50
Squamous cell carcinoma	39	31
Large cell carcinoma	4	3
NSCLC (not otherwise specified)	20	16
Chemotherapy (concurrent/sequential)	87(63/24)	69
Chemotherapy regimens		
Cisplatin + vindesine or vinorelbine	48	55
Carboplatin + paclitaxel	12	14
MVP (cisplatin + vindesine + mitomycin)	12	14
Nedaplatin or nedaplatin + paclitaxel	11	13
Others	4	5

When evaluating overall survival, an event was defined as death from any cause. When evaluating progression-free survival, an event was defined as documented tumor progression (loco-regional or distant) or death from any cause. Local or loco-regional failure was judged to have occurred if there was radiographic evidence of progressive disease. Absence of progression of residual disease for more than 6 months following treatment was considered evidence of loco-regional control. A recurrence in supraclavicular nodes was considered regional failure, not an elective nodal failure, because the supraclavicular regions are not routinely included within the radiation fields in our practice. Treatment failure was not always confirmed histologically. Elective nodal failure (ENF) was defined as recurrence in CTVs without evidence of local failure, as the first event or even after distant metastasis.

The adequacy of field borders was assessed in terms of CTVs coverage and PTV margin in patients with loco-regional failure. The failure patterns were analyzed to distinguish in-field recurrence from out-of-field recurrence; "in-field" included CTVs as well as CTVp and CTVn.

The Kaplan–Meier method was used from the start of the treatment to calculate the overall survival and progression-free survival of all the 127 patients.

Results

A total of 127 patients, median age 65 years (range, 36–83), met the criteria for evaluation in this study. The majority of patients had stage IIIA ($n = 59$) or IIIB ($n = 51$) disease. Other baseline characteristics of the patients and details of their treatment are summarized in Table 1.

At a median follow-up time of 50.5 months (range, 14.2–83.0) of the surviving patients, 95 had experienced treatment failure. Median survival time was 23.5 months (range, 4.2–109.7), and median time to progression was 9.0 months (range, 2.2–109.7). The 2-year cumulative survival rate and 2-year progression-free survival rate were 51.4% and 27.6%, respectively. The survival

curves are shown in Fig. 1. Patients with early progressions were excluded because of the criteria for inclusion in this study: a clinical response better than stable disease.

Eighty-seven (69%) patients received chemotherapy concomitantly or sequentially with the radiotherapy. The overall survival time of the patients who received chemotherapy was 21.7 months (range, 7.6–33.9), as opposed to 19.1 months (range, 6.8–32.7) among those who did not receive chemotherapy, and the difference was not statistically significant ($p = 0.10$). There were no statistically significant differences in disease-free survival nor loco-regional control according to whether the patients had received chemotherapy. Concurrent use of chemoradiotherapy did not affect survival among the 87 patients who received chemotherapy (data not shown).

There were 53 patients with a first loco-regional failure, alone ($n = 41$) or with distant metastasis ($n = 12$), and the majority of the failures were in-field ($n = 38$, 72%). Nine (21%) patients had out-of-field recurrences in the form of supraclavicular node metastasis ($n = 5$) or pleural metastasis ($n = 4$), with or without local recurrence. There were no isolated ENFs (Table 2).

Four patients (7%) experienced nodal failure in CTVs simultaneously with local or distant failure. Three of them had received a prophylactic dose of 40 Gy to the CTVs, and the other had inadequate margin of the CTVs field. Other characteristics of these patients are shown in Table 3. There were no "marginal only" failures among in-field failures; all the failures at the field borders were associated with out-of-field failures.

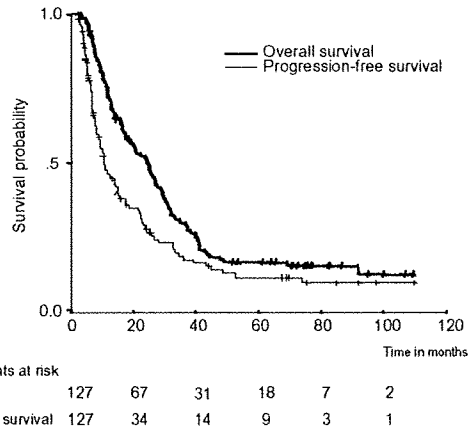

Fig. 1. Overall and progression-free survival curves of all the 127 patients. Patients with early progressions were excluded because of the criteria for inclusion in this study: a clinical response better than stable disease.

Table 2
Details of all the first failures.

Types of event	Patients	%
Loco-regional alone	41	43%
In-field		
CTVpn	30	
CTVpn + CTVs[a]	2	
In-field + out-of-field		
CTVpn + pleural effusion	2	
CTVpn + supraclavicular nodes	2	
Out-of-field		
Supraclavicular nodes	3	
Pleural effusion[b]	2	
Loco-regional + distant	12	13%
In-field + out-of-field		
CTVpn + CTVs	2	
Distant alone	42	44%
All events	95	

[a] One also had concurrent failure in the contralateral hilum.
[b] One also had concurrent supraclavicular recurrence.

Conventional X-ray simulation was performed in 8 (6%) patients, while 70 (55%) had CT-based simulation and remaining 49 (39%) had both (initially with X-ray simulation, followed by CT-based simulation for off-cord boost). A majority ($n = 122$, 96%) of the patients were treated with anteroposterior opposing fields as elective nodal irradiation, followed by oblique opposing fields to the total dose.

ENI was incomplete ($n = 12$) or not performed ($n = 6$) in 18 of the 53 patients with loco-regional failure because of diminished pulmonary function or deteriorated performance status. All the incomplete ENIs were due to insufficient CTVs coverage. In 12 of the 18 patients, the failure was in the tumor volume, in 3 patients it was in the pleura, and in 2 patients it was in the supraclavicular nodes. Only 1 patient had recurrence in both the tumor volume and the uninvolved nodal area.

Discussion

In this series of NSCLC cases treated with conventional fields and doses, the loco-regional failures after radiotherapy mainly occurred in the tumor volumes, and there were no isolated ENFs.

There are several possible reasons for these results. First, micrometastasis in the CTVs may have been controlled by prophylactic delivery of 40 Gy to the region, and depending on the location of the primary tumor, the sites of occult metastasis may often have received additional unintentional radiation doses. Kepka et al. reported an isolated ENF rate of 9% in 185 patients treated with the ENI using 3-dimensional conformal radiotherapy (3D-CRT). Their analysis showed that the ENF occurred more frequently in the regions that received under 40 Gy than in the regions that received higher doses (69% vs. 31%, respectively, $p = 0.04$) [7]. However, despite the same ENF rate of 9% in 1705 patients in the four trials conducted by the Radiation Therapy Oncology Group (RTOG), a retrospective evaluation of in-field progression revealed that neither in-field progression nor survival was affected by the adequacy of ENI [8]. Field adequacy did not have any negative impact on regional control in our series either (Tables 3).

Second, the amount of micrometastasis in unenlarged mediastinal regional nodes may have been small enough to be controlled by chemotherapy, which has been shown to have activity that reduces the incidence of distant micrometastasis in advanced NSCLC. However, the degree of systemic and local efficacy of chemotherapy did not reach statistical significance in our series, probably because of the small number of patients and their heterogeneity (data not shown).

Third, since the failure sites in the majority of patients were distant, they would have died of their disease before the ENF became apparent. As a result, the loco-regional failure rates may have been lower than their true values because we did not investigate regional sites once a patient developed distant metastasis.

The therapeutic significance of treating subclinical nodal regions during and after surgery for NSCLC has been questioned. Some studies have established the presence of considerable microscopic nodal disease in clinically uninvolved lymph nodes [9,10], but the role of mediastinal lymphadenectomy remains controversial and has been limited to the precise staging of the disease [11–13]. A study by Izbicki et al. which compared systemic mediastinal lymphadenectomy with mediastinal lymph node sampling showed that radical systemic mediastinal lymphadenectomy had no effect on the disease-free or overall survival of patients with limited nodal involvement [13,14]. The role of adjuvant radiotherapy after complete resection also remains unclear [15–17]. A systemic

Table 3
Patients with CTVs failure.

	Patient #1	Patient #2	Patient #3	Patient #4
Age (yr)/Sex	45/Female	74/Female	61/Male	78/Male
Reason for inoperability	Unresectable	Unresectable	Decreased pulmonary function	Unresectable, age
Stage	IIIA	IIIA	IIB	IIIB
Primary location	Left lower lobe	Right upper lobe	Right lower lobe	Left upper lobe
Histology	Adenocarcinoma	Adenocarcinoma	Squamous cell carcinoma	Adenocarcinoma
Chemotherapy	Yes	Yes	No	No
Response	Partial response	Partial response	Partial response	Partial response
Site of first failure	Distant and loco-regional	Distant and loco-regional	Loco-regional	Loco-regional
Field border adequacy	Yes	Yes	No	Yes
Dose to CTVs failure	40	40	0	40
Death	No	No	Yes	No

review and meta-analysis [18] showed that postoperative radiotherapy was detrimental to patients with early NSCLC, although there may have been some efficacy in patients with N2 tumors. These arguments also raise questions about the clear benefit of ENI in regard to survival.

In-field loco-regional failure was a major site of failure in the current study: all the recurrences in the CTVs were associated with failure in the gross tumor volume. Thus, more intensive treatment strategies are needed to enhance loco-regional control without sacrificing safety. One possible strategy is to reduce the ENI field in regard to the patients' risk factors while escalating the total dose. Such an attempt has already been made in regard to surgery: Asamura et al. retrospectively reviewed the prevalence of lymph node metastasis with respect to the location of the primary tumor or other characteristics to decide on the optimal lobe-specific extent of systematic lymph node dissection for NSCLC [19,20]. By using such predictors, including the location of the primary tumor, histology, or nodal stage [21–24], it is possible to identify the nodal areas at risk and to optimize the extent of ENI in radiation therapy as well. On the other hand, more precise diagnosis by novel technology, such as positron emission tomography [25], may enable the omission of ENI and avoid unnecessary irradiation to areas at low risk for subclinical disease.

In terms of the technical feasibility of dose escalation, Grills et al. found that intensity-modulated radiation therapy without ENI for NSCLC increased the deliverable mean target dose in node-positive patients by 25–30% over 3D-CRT and by 130–140% over traditional ENI [26].

Because omitting ENI is likely to leave microscopic disease untreated, there is concern that it may result in increased failure in these areas. However, the preliminary results of dose escalation trials have shown that isolated ENF outside the irradiated volume occurred in fewer than 6% of the cases and that omission of ENI did not seem to sacrifice outcome [2–5,27]. There is insufficient evidence to support the use of ENI for any patient with localized NSCLC (Stages I–III), irrespective of whether chemotherapy is administered [28]. There has been only one randomized trial that compared high-dose thoracic radiotherapy without ENI and standard dose radiotherapy with ENI, and it showed a survival benefit of high-dose thoracic radiotherapy without ENI [29]. One possible explanation for this finding is that incidental doses to elective nodal areas may contribute to the eradication of the subclinical disease. The pattern of ENF according to nodal regions was described by Rosenzweig et al., who implemented the use of involved-field radiation therapy with dose escalation in 524 patients [6]. Since the majority of the 42 ENFs that were observed occurred in the areas that received less than 45 Gy, the incidental doses to elective nodal areas may have been substantial despite the attempt not to treat these regions in their study. In addition, Zhao et al. reported that involved-field radiation therapy with a dose escalated to 70 Gy delivered a considerable dose to CTVs, and when the primary tumor was large or centrally located, the percentages of CTVs in the lower paratracheal region, subcarinal region and ipsilateral hilar region receiving over 40 Gy were 33%, 39%, and 98%, respectively [30].

Because of the retrospective nature of our study, no conclusions about the value of ENI for NSCLC can be drawn. However, the finding that in-field loco-regional failure, as well as distant metastasis, was a major type of failure with the standard field and dose of thoracic radiotherapy confirmed the need for more intensive treatment.

Further investigation to verify the true significance of ENI or to identify best candidates for ENI is necessary before it is abandoned in the context of dose escalation.

Conclusion

The loco-regional failures after radiotherapy in this series of NSCLC cases treated with conventional fields and doses mainly occurred in the tumor volumes, and there were no isolated ENFs. The results confirmed the need for more intense treatment to improve local control.

References

[1] Penland SK, Socinski MA. Management of unresectable stage III non-small cell lung cancer: the role of combined chemoradiation. Semin Radiat Oncol 2004;14:326–34.
[2] Belderbos JS, De Jaeger K, Heemsbergen WD, et al. First results of a phase I/II dose escalation trial in non-small cell lung cancer using three-dimensional conformal radiotherapy. Radiother Oncol 2003;66:119–26.
[3] Rosenman JG, Halle JS, Socinski MA, et al. High-dose conformal radiotherapy for treatment of stage IIIA/IIIB non-small-cell lung cancer: technical issues and results of a phase I/II trial. Int J Radiat Oncol Biol Phys 2002;54:348–56.
[4] Socinski MA, Morris DE, Halle JS, et al. Induction and concurrent chemotherapy with high-dose thoracic conformal radiation therapy in unresectable stage IIIA and IIIB non-small-cell lung cancer: a dose-escalation phase I trial. J Clin Oncol 2004;22:4341–50.
[5] Wu KL, Jiang GL, Liao Y, et al. Three-dimensional conformal radiation therapy for non-small-cell lung cancer: a phase I/II dose escalation clinical trial. Int J Radiat Oncol Biol Phys 2003;57:1336–44.
[6] Rosenzweig KE, Sura S, Jackson A, et al. Involved-field radiation therapy for inoperable non small-cell lung cancer. J Clin Oncol 2007;25:5557–61.
[7] Kepka A, Szajda SD, Jankowska A, et al. Risk of isolated nodal failure for non-small cell lung cancer (NSCLC) treated with the elective nodal irradiation (ENI) using 3D-conformal radiotherapy (3D-CRT) techniques – A retrospective analysis. Acta Oncol 2008;47:95–103.
[8] Emami B, Mirkovic N, Scott C, et al. The impact of regional nodal radiotherapy (dose/volume) on regional progression and survival in unresectable non-small cell lung cancer: an analysis of RTOG data. Lung Cancer 2003;41:207–14.
[9] Izbicki JR, Passlick B, Hosch SB, et al. Mode of spread in the early phase of lymphatic metastasis in non-small-cell lung cancer: significance of nodal micrometastasis. J Thorac Cardiovasc Surg 1996;112:623–30.
[10] Oda M, Watanabe Y, Shimizu J, et al. Extent of mediastinal node metastasis in clinical stage I non-small-cell lung cancer: the role of systematic nodal dissection. Lung cancer 1998;22:23–30.
[11] Keller SM, Adak S, Wagner H, et al. Mediastinal lymph node dissection improves survival in patients with stages II and IIIa non-small cell lung cancer. Eastern Cooperative Oncology Group. Ann Thorac Surg 2000;70:358–65 [discussion 365–366].
[12] Sugi K, Nawata K, Fujita N, et al. Systematic lymph node dissection for clinically diagnosed peripheral non-small-cell lung cancer less than 2 cm in diameter. World J Surg 1998;22:290–4 [discussion 294–295].

[13] Izbicki JR, Passlick B, Pantel K, et al. Effectiveness of radical systematic mediastinal lymphadenectomy in patients with resectable non-small cell lung cancer: results of a prospective randomized trial. Ann Surg 1998;227:138–44.
[14] Izbicki JR, Thetter O, Habekost M, et al. Radical systematic mediastinal lymphadenectomy in non-small cell lung cancer: a randomized controlled trial. Br J Surg 1994;81:229–35.
[15] Dautzenberg B, Arriagada R, Chammard AB, et al. A controlled study of postoperative radiotherapy for patients with completely resected non-small cell lung carcinoma. Groupe d'Etude et de Traitement des Cancers Bronchiques. Cancer 1999;86:265–73.
[16] Keller SM, Adak S, Wagner H, et al. A randomized trial of postoperative adjuvant therapy in patients with completely resected stage II or IIIA non-small-cell lung cancer. Eastern Cooperative Oncology Group. N Engl J Med 2000;343:1217–22.
[17] Trodella L, Granone P, Valente S, et al. Adjuvant radiotherapy in non-small cell lung cancer with pathological stage I: definitive results of a phase III randomized trial. Radiother Oncol 2002;62:11–9.
[18] Rowell NP. Postoperative radiotherapy in non-small-cell lung cancer. Lancet 1998;352:1384 [author reply 1385–1386].
[19] Asamura H, Nakayama H, Kondo H, et al. Lobe-specific extent of systematic lymph node dissection for non-small cell lung carcinomas according to a retrospective study of metastasis and prognosis. J Thorac Cardiovasc Surg 1999;117:1102–11.
[20] Asamura H, Nakayama P, Kondo H, et al. Lymph node involvement, recurrence, and prognosis in resected small, peripheral, non-small-cell lung carcinomas: are these carcinomas candidates for video-assisted lobectomy? J Thorac Cardiovasc Surg 1996;111:1125–34.
[21] Komaki R, Scott CB, Bymandt R, et al. Failure patterns by prognostic group determined by recursive partitioning analysis (RPA) of 1547 patients on four radiation therapy oncology group (RTOG) studies in inoperable nonsmall-cell lung cancer (NSCLC). Int J Radiat Oncol Biol Phys 1998;42:263–7.
[22] Komaki R, Scott CB, Sause WT, et al. Induction cisplatin/vinblastine and irradiation vs. irradiation in unresectable squamous cell lung cancer: failure patterns by cell type in RTOG 88-08/ECOG 4588. Radiation Therapy Oncology Group. Eastern Cooperative Oncology Group. Int J Radiat Oncol Biol Phys 1997;39:537–44.
[23] Movsas B, Scott C, Sause W, et al. The benefit of treatment intensification is age and histology-dependent in patients with locally advanced non-small cell lung cancer (NSCLC): a quality-adjusted survival analysis of radiation therapy oncology group (RTOG) chemoradiation studies. Int J Radiat Oncol Biol Phys 1999;45:1143–9.
[24] Suzuki K, Nagai K, Yoshida J, et al. Clinical predictors of N2 disease in the setting of a negative computed tomographic scan in patients with lung cancer. J Thorac Cardiovasc Surg 1999;117:593–8.
[25] Vansteenkiste J, Fischer BM, Booms C, et al. Positron-emission tomography in prognostic and therapeutic assessment of lung cancer: systematic review. Lancet Oncol 2004;5:531–40.
[26] Grills IS, Yan D, Martinez AA, et al. Potential for reduced toxicity and dose escalation in the treatment of inoperable non-small-cell lung cancer: a comparison of intensity-modulated radiation therapy (IMRT), 3D conformal radiation, and elective nodal irradiation. Int J Radiat Oncol Biol Phys 2003;57:875–90.
[27] Senan S, Burgers S, Samson MJ, et al. Can elective nodal irradiation be omitted in stage III non-small-cell lung cancer? Analysis of recurrences in a phase II study of induction chemotherapy and involved-field radiotherapy. Int J Radiat Oncol Biol Phys 2002;54:999–1006.
[28] Senan S, De Ruysscher D, Girand P, et al. Literature-based recommendations for treatment planning and execution in high-dose radiotherapy for lung cancer. Radiother Oncol 2004;71:139–46.
[29] Yuan S, Sun X, Lim L, et al. A randomized study of involved-field irradiation versus elective nodal irradiation in combination with concurrent chemotherapy for inoperable stage III nonsmall cell lung cancer. Am J Clin Oncol 2007;30:239–44.
[30] Zhao L, Chen M, Ten Haken R, et al. Three-dimensional conformal radiation may deliver considerable dose of incidental nodal irradiation in patients with early stage node-negative non-small cell lung cancer when the tumor is large and centrally located. Radiother Oncol 2007;82:153–9.

CI研究30 (3・4):115-121, 2008

Multimodality 画像を用いた脳腫瘍の手術戦略
—脳腫瘍手術における解剖学的・生理学的脳機能評価法の臨床的意義—

三國 信啓　菊池 隆幸　松本 敦仁
横山 洋平　高橋 潤　橋本 信夫

Clinical Impact of Anatomo-functional Evaluation of Brain Function during Brain Tumor Surgery

Nobuhiro Mikuni, Takayuki Kikuchi, Atsushi Matsumoto, Yohei Yokoyama,
Jun Takahashi, and Nobuo Hashimoto

Department of Neurosurgery, Kyoto University Graduate School of Medicine, Kyoto, Japan

(*Received August 4, 2008*)
(*Accepted November 4, 2008*)

Summary: To attempt to improve surgical outcome of brain surgery, clinical significance of anatomo-functional evaluation of brain function during resection of brain tumors was assessed.

Seventy four patients with glioma located near eloquent areas underwent surgery while awake. Intraoperative tractography-integrated functional neuronavigation and cortical/subcortical electrical stimulation were correlated with clinical symptoms during and after resection of tumors.

Cortical functional areas were safely removed with negative electric stimulation and eloquent corticies could be removed in some circumstances. Subcortical functional mapping was difficult except for motor function.

Studying cortical functional compensation allows more extensive removal of brain tumors located in the eloquent areas.

Key Words: Brain function, Glioma, Awake surgery
使用機種: Vector Vision Compact Navigation System, Brain LAB AG, Heimstetten, Germany, Epoch XP, Axon Systems, NY, USA

序　文

脳腫瘍，とくにグリオーマの治療成績を向上させうる治療として様々な取り組みが注目されている．放射線治療と組み合わせた化学療法は病態別にプロトコールを検討されるようになり，遺伝子治療・細胞療法・分子標的療法・免疫療法においてはそれぞれの臨床的位置づけが確立されつつあり，新たな集学的治療の大系が作成されつつある．手術治療に関しては「より多く」摘出することが予後と関係し[9]，摘出度の術中評価には蛍光色素や術中MRIの導入が行われている．「より安全に」という前提条件をいかに術前あるいは術中に満たせるか，という課題についても臨床，基礎研究が進んでいる．各種非侵襲的脳機能評価，高次場MRIに術前情報を載せた術中navigation systemと脳表・深部白質の電気刺激との融合，さらに覚醒下手術を用いることにより，脳機能のマッピング・モニタリングはもとより，その可塑性の研究も可能となる[2]．

我々は脳腫瘍という病態下での脳機能について，機能野皮質およびその連絡神経線維の同定あるいは定義，と機能部位摘出か温存かの判断の根拠となりうる代償機構について研究を進めている．Diaschisis，行動的補償，適応的可塑性といった代償機構のメカニズムを持つ脳機能の研究は神

京都大学医学研究科 脳神経外科【連絡先：〒606-8507 京都市左京区聖護院川原町54】

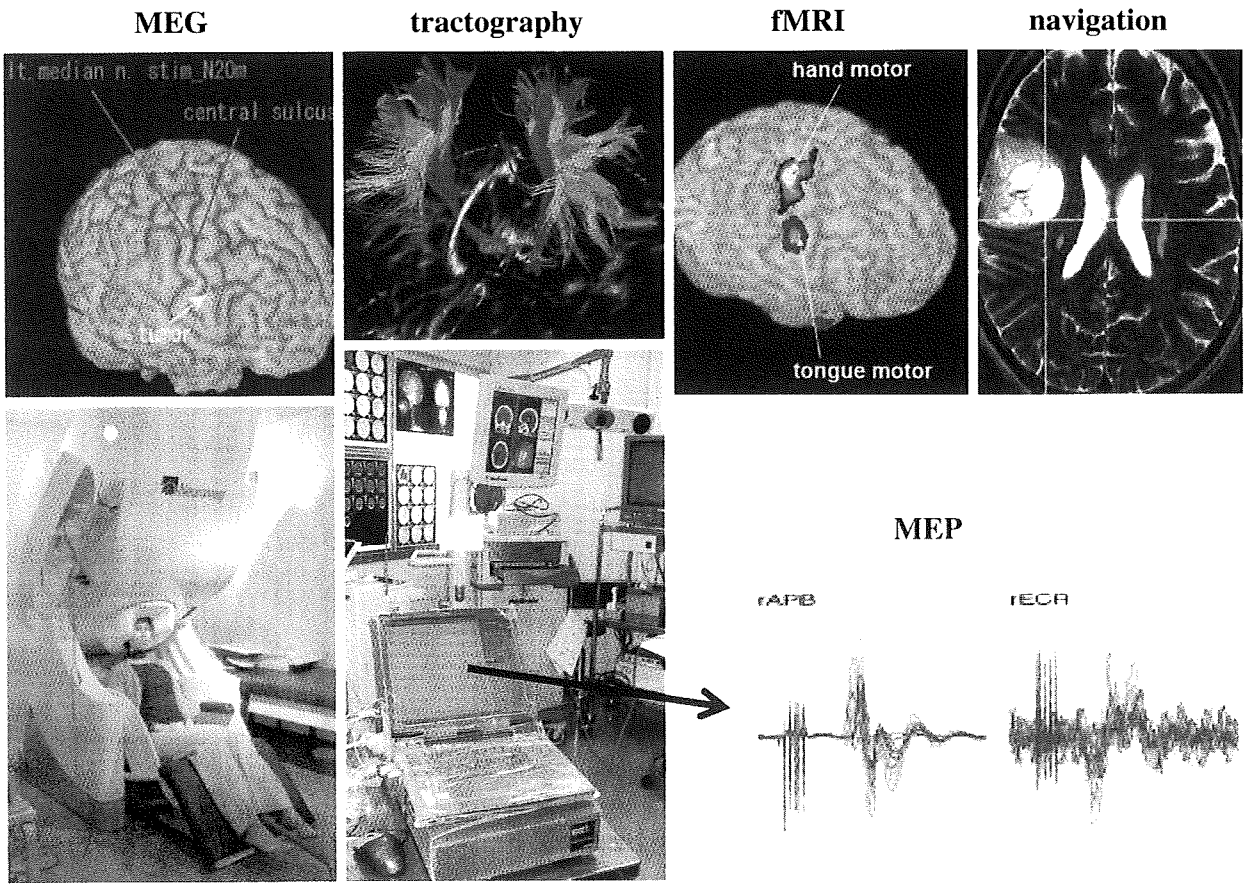

Fig. 1　Functional neuronavigation of cortical information in a patient with a diffuse astrocytoma in the right precentral gyrus. Results of magnetoencephalography (MEG) , DTI tractography, and functional magnetic resonance image (fMRI) were integrated into an intraoperative neuronavigation system (navigation; cross of yellow lines indicates real position of probe, red dots are pyramidal tracts according to the results of DTI tractography) then were confirmed with electrophysiological evaluation (motor evoked potential; MEP; *right bottom*) .

経科学としても興味深いが，脳腫瘍の外科治療における重要なテーマであると考えている．本稿では脳腫瘍治療において脳機能部位摘出を含めた拡大摘出のために必要な，脳機能評価，つまりDTIトラクトグラフィーを導入したfunctional neuronavigationと術中皮質白質電気刺激，覚醒下随意活動を同時に用いた術中脳機能評価法の臨床的意義について検討した結果を報告する．

方　法

脳機能部位近傍の脳腫瘍の摘出を覚醒下にて行った74例（年齢15–69歳）を対象とした．全例で術前拡散テンソル画像によるtractographyを作成し術中navigation表示し，皮質白質電気刺激を行った．脳機能部位術前同定には3T MRIによる解剖学的位置を参考にして，機能的MRI(fMRI)および脳磁図(MEG)の結果を合わせてtractographyを作成した(functional neuronavigation)(**Fig. 1**)．病変部そのものの皮質電気刺激による陰性あるいは陽性反応出現時に摘出を行うかどうかは症例ごとに検討した．我々の用いている白質での電気刺激ではneuronavigation上の神経線維まで術中に1センチの距離となれば刺激が必要であり[4]，陰性あるいは陽性反応出現時には刺激部位から最大7ミリまでに神経線維が存在する[6]ために原則摘出を中止した(**Fig. 2**)．術中覚醒下手術および皮質白質電気刺激は倫理委員会の承諾と患者の同意を得て行った．

結　果

皮質電気刺激による陽性運動反応は第4野，第6aα，6aβ野，第8野から65例で，陰性運動反応は26例で第6aα，6aβ野を中心に第44野刺激時にも認めた．異常感覚症状は主に第3，1，2野に38例で認め，2次性体性感覚野(第5，7野)で生じることもあった．言語反応では呼称障害が最も多く32例で出現しその範囲は，Broca野やWernicke野を越

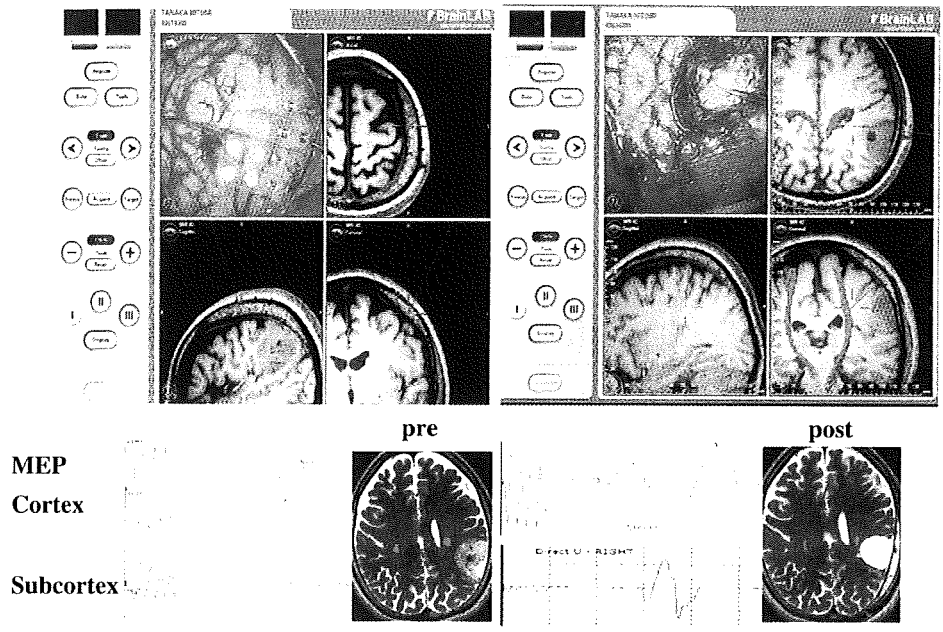

Fig. 2 Clinical impact of integrated functional neuronavigation and cortical, subcortical electrical stimulation to preserve motor function during the resection of left parietal glioma. (**Left**) Before resection, precentral gyrus elicited motor evoked potential (**MEP Cortex**; *bottom green line*) by electrical stimulation. (**Right**) During resection of the tumor, subcortex close to the pyramidal tract fiber tracking (*top of green line*) elicited MEP (**MEP subcortex**) at the end of resection. Preoperative (**Pre**) and postoperative (**Post**) T2-weighted MR images with pyramidal tract fiber tracking (*red dots*) showed that the tumor, close to the pyramidal tracts, was totally removed.

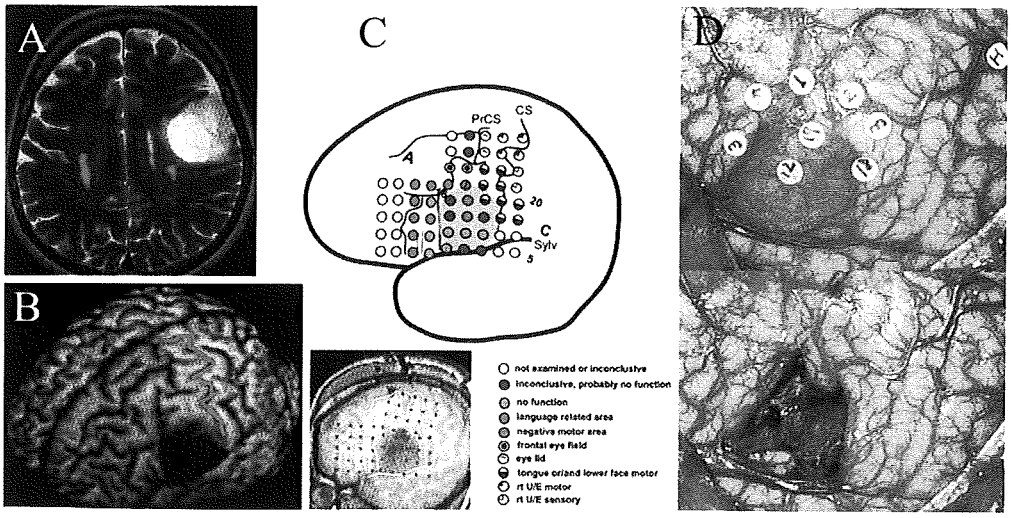

Fig. 3 MRIs and functional localization with chronic subdural electrodes on language-dominant frontal lobe. (**A**) A 53-year-old woman suffered from a left frontal diffuse astrocytoma. (**B**) The tumor was located close to the central sulcus (*red line*) and the language area. (**C**) Elecric stimulation showed that language area (*red circles*) and negative motor area (*green circles*) was included in the tumor. (**D**) Removal of parts of the language area and negative motor areas did not cause neurological deficits.

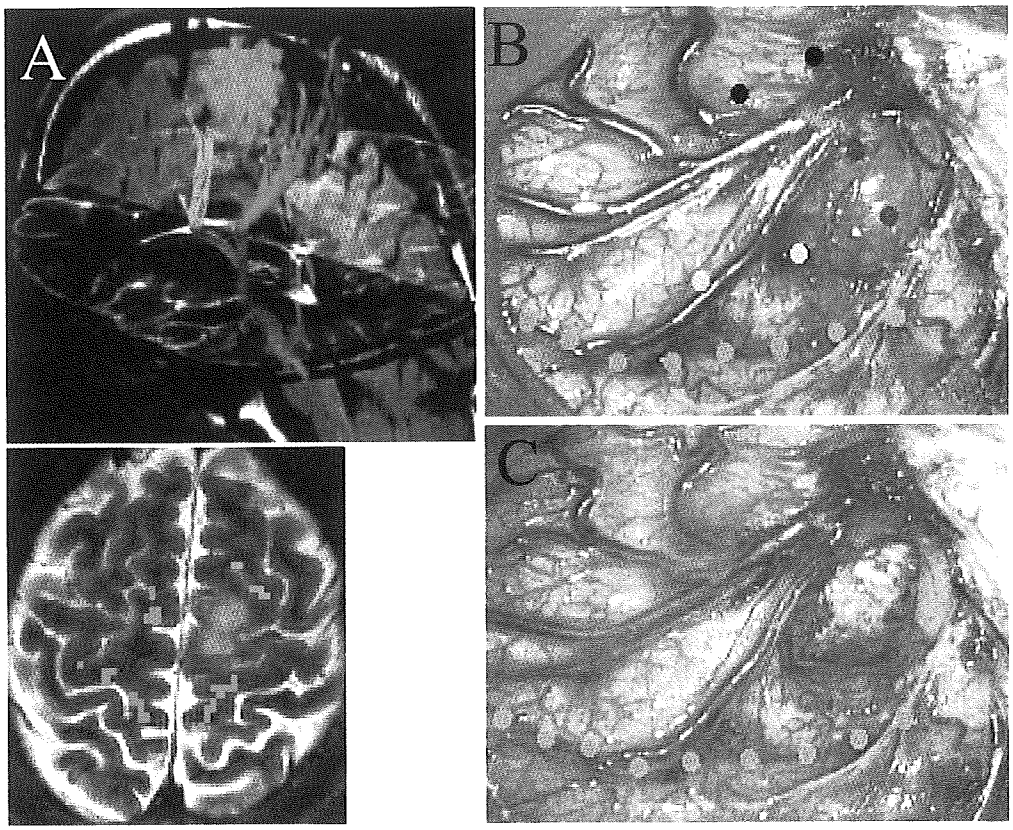

Fig. 4　Removal of functional cortex in a 23-year-old man with diffuse astrocytoma located at the left precentral gyrus. (**A**) Preoperative DTI tractography showed that the tumor was located close to the pyramidal tracts (*red lines*). (**B**) Intraoperative electric stimulation on the tumor elicited motor evoked potentials (MEPs) in quadriceps (*blue dots*) and biceps (*yellow dots*) muscles. (**C**) Tumor was removed with transient slight motor weakness in his right arm. Green dots: central sulcus defined by SEP

えて言語優位側の側頭葉，前頭葉，頭頂葉に及ぶ広範囲で生じ，また島表面での電気刺激でも観察された．頭頂葉では14例でGerstmann症候群の一部や失行が出現し，後頭葉では5例で陽性の明視反応が電気刺激時に生じた．顔面の運動野は摘出可能であるが，その他の脳機能が存在する皮質の摘出において18例で計画的に施行し，急性期機能障害を12例で生じたがいずれも3ヶ月以内に消失した（**Fig. 3, 4**）．

白質電気刺激による陽性運動反応はほぼ全例で，術中navigation上のcortico spinal tracts近傍1センチ以内の刺激時に得られた．一方で感覚野からの神経線維，弓状束，視覚路のtractography近傍1センチ以内の白質刺激時では，異常感覚，言語障害，明視感の発現はそれぞれ78%，40%，20%であった．白質障害と考えられる永続する症状として感覚異常を1例で，言語障害を3例で認めた（**Fig. 5**）．術前より中等度運動麻痺のある患者では，覚醒下での神経症状のモニタリングが最も有用であった[5]（**Fig. 6**）．

考　察

「脳機能野」は解剖学的病理学的あるいは生理学的に同定されるがその局在結果は簡単には一致しない．さらに，生理学的検査の中でも脳波や脳磁図といった脳細胞の電気生理活動とfMRIやPETが示す脳細胞血流代謝は関連してはいるものの，評価している対象や活動時期が異なる．同じ電気生理学的検索でも検査のタスク種類によって活動する脳の部位が異なる[1]．我々の施設では，てんかん症例における硬膜下電極留置を使用した脳機能マッピングの経験が豊富であり，脳電気刺激による機能野同定を「脳機能部位」の定義としている．

運動に関してBrodmannの第4野と第6aα野を生理学的に分けることはしばしば困難であり，電気刺激による手の陽性運動反応出現部位はさらに前方の第6aβ野まで広が